

dc- and ac-magnetic field-induced strain effects in ferromagnetic shape memory composites of Ni–Mn–Ga single crystal and polyurethane polymer

Min Zeng,^{1,2} Siu Wing Or,^{2,a)} and Helen Lai Wa Chan¹

¹Department of Applied Physics, The Hong Kong Polytechnic University, Hung Hom, Kowloon, Hong Kong

²Department of Electrical Engineering, The Hong Kong Polytechnic University, Hung Hom, Kowloon, Hong Kong

(Presented 19 January 2010; received 31 October 2009; accepted 21 December 2009; published online 4 May 2010)

Ferromagnetic shape memory composites of multilayer and sandwich types were fabricated by laminating Ni–Mn–Ga single-crystal plates with polyurethane (PU) polymer plates. The dc- and ac-magnetic field-induced strains (MFISs) in the composites were measured as functions of both magnetic field and mechanical load, and the results were compared with those of the single crystal. It was found that the load-free dc-MFISs were 5.6%, 1.5%, and 0.8%, while the load-free ac-MFISs were 0.3%, 0.8%, and 0.5% in the single crystal, multilayer composite, and sandwich composite, respectively. The relatively smaller load-free dc-MFISs and larger load-free ac-MFISs in the composites than the single crystal originated from the stress bias of the Ni–Mn–Ga plates by the PU plates in the composites. The dc-MFISs of all samples and the ac-MFISs of the composites decreased with the increase in mechanical load amplitude, while the ac-MFIS of the single crystal peaked at 1.6 MPa load. © 2010 American Institute of Physics. [doi:10.1063/1.3357408]

Ferromagnetic shape memory (FSM) alloys, which exhibit giant magnetic field-induced strains (MFISs) in the martensitic phase, have attracted increasing research interest due to their potential applications in new generation actuation and transduction devices.^{1–6} Since the discovery of 0.19% dc-MFIS in Ni₂MnGa single crystal at –8 °C in 1996,¹ there have been reports of several FSM alloy systems such as Ni–Mn–Ga, Co–Ni–Al, Ni–Ga–Fe, Fe–Pd, Fe–Pt, etc.^{2–6} Among them, dc-MFISs of as large as 6% and 10% have been found, respectively, in the tetragonal and orthorhombic martensitic phases of Ni–Mn–Ga single crystals in load-free condition at room temperature.^{2,3} Importantly, these values are close to the theoretical maximum lattice strain given by $1 - c/a$ in the respective martensitic phase, and the mechanism of giant MFISs is a reorientation of martensitic twin variants under an applied magnetic field.^{2,3} In other words, as the martensitic twin variants are orthogonal to each other, the twin variants with their easy (c) axis of magnetization favorably oriented in the applied magnetic field direction grow at the expense of the others, resulting in a reorientation of twin variants.

Although Ni–Mn–Ga single crystals exhibit giant dc-MFISs, they have very limited strain recovery capability upon removal of the applied magnetic field, leading to small ac-MFISs and large remanent strains.⁷ By applying a magnetic field normal to the original magnetic field direction or a mechanical load parallel to the sample's elongation direction, it can effectively reset the reoriented twin variants back to their original state.^{2,7,8} However, an additional resetting means is required, adding complications to the device design and fabrication. A possible approach is to combine the Ni–

Mn–Ga single crystals with a passive polymer to form composites.⁹ The polymer in the composites not only prevents the brittle Ni–Mn–Ga from being damaged but also provides an internal stress bias to restore the Ni–Mn–Ga based on an elastic shrinkage stress induced in the polymer during actuation of the Ni–Mn–Ga. Previous research on the actuation properties of the Ni–Mn–Ga-based composites only dealt with the dc-MFIS effect.⁹ In this work, the combined dc- and ac-MFIS effects are reported in both multilayer and sandwich composites formed by Ni–Mn–Ga single-crystal plates and polyurethane (PU) polymer plates. The results are compared with the single crystal and discussed in terms of reorientation and configuration of martensitic twin variants under applied magnetic field and mechanical load.

Figure 1 shows the schematic diagrams of Ni–Mn–Ga single crystal and its multilayer and sandwich composites, detailing the crystallographic orientation of the single crystal, the structure of the composites, and the directions of the

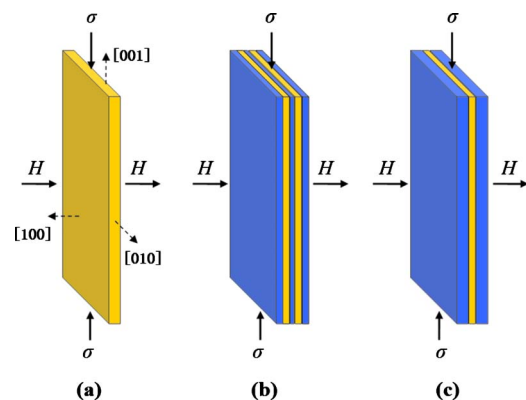


FIG. 1. (Color online) Schematic diagrams of (a) Ni–Mn–Ga single crystal, (b) multilayer composite, and (c) sandwich composite.

^{a)}Author to whom correspondence should be addressed. Electronic mail: eeswor@polyu.edu.hk.

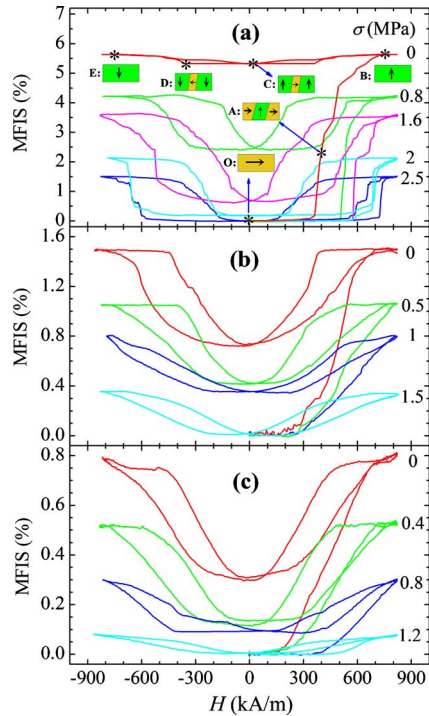


FIG. 2. (Color online) MFISs of (a) Ni–Mn–Ga single crystal, (b) multilayer composite, and (c) sandwich composite under different applied mechanical loads (σ) for the first one and a quarter cycles of the applied magnetic field (H). Various illustrations depicting the evolution of twin variants at load-free condition are also included in (a) for the single crystal.

applied magnetic field (H) and mechanical load (σ) for magnetomechanical testing. The lighter regions denote the Ni–Mn–Ga plates, while the darker regions represent the PU plates.

The Ni–Mn–Ga plates, with a chemical composition of $\text{Ni}_{50}\text{Mn}_{29}\text{Ga}_{21}$, dimensions of $19.5^L \times 5^W \times 1.1^T$ mm³ (where L =length, W =width, and T =thickness), the two major surfaces parallel to the $\{011\}$ plane, and a load-free dc-MFIS of 5.6% at room temperature, were provided by AdaptaMat, Ltd., in Finland. The transformation temperatures were determined to be austenite start (A_s)=38 °C, austenite finish (A_f)=41 °C, martensite start (M_s)=35 °C, and martensite finish (M_f)=33 °C using a differential scanning calorimeter (PerkinElmer DSC7). The martensitic structure was found to be nearly tetragonal with the lattice parameters of $a=b=0.594$ nm and $c=0.560$ nm by an x-ray diffractometer (Bruker AXS D8 Advance), giving the theoretical maximum lattice strain ($\epsilon_0=1-c/a$) of 5.7%. The easy (c) and hard (a and b) axes of magnetization were along the $[001]$ and $[100]/[010]$ directions, respectively, while the magnetocrystalline anisotropy constant (K_μ) was 176 kJ/m³, as evaluated from the magnetization-field (M - H) curves using a vibrating sample magnetometer (Lakeshore 7600). The PU plates, having dimensions of $19.5^L \times 5^W \times 0.73^T$ or 1.65^T mm³ and with a low elastic modulus (E_p) of 28 MPa, were prepared from a three-component resin system supplied by DuPont, China, with the trade name Terathane. To preset an initial nearly single-variant state in the composites, the length of the Ni–Mn–Ga plates was maximally shortened by applying a dc magnetic field of 1 T along their length direction. Keeping

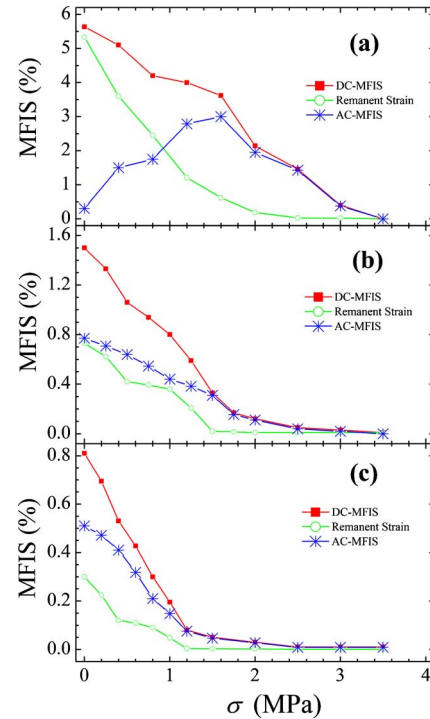


FIG. 3. (Color online) Dependences of dc-MFIS, remanent strain, and ac-MFIS on the applied mechanical load (σ) for (a) Ni–Mn–Ga single crystal, (b) multilayer composite, and (c) sandwich composite.

the field unchanged, bonding of the Ni–Mn–Ga plates with the PU plates of an appropriate thickness was performed at room temperature to avoid the presence of austenitic phase in the Ni–Mn–Ga plates. The resulting multilayer and sandwich composites had the same dimensions of $19.5^L \times 5^W \times 4.4^T$ mm³ but with different Ni–Mn–Ga volume fractions (v) of 0.5 and 0.25, respectively.

The magnetomechanical testing was performed using a setup built in-house. A mechanical load (σ) was supplied by energizing a spring actuator toward the sample under test along the $[001]$ direction. An electromagnet driven by a dynamic signal analyzer (Ono Sokki CF5220) via a power-supply amplifier (Techron TEC7572) was used to produce a sinusoidal magnetic field (H) of 820 kA/m (peak) at a frequency of 0.1 Hz in the $[100]$ direction. A Hall probe situated adjacent to the sample and connected to a gaussmeter (F. W. Bell 7030) was employed to monitor H . The MFIS from the sample was measured by a laser displacement sensor (Keyence LK-G82) connected to a controller (Keyence LK-G3001) with a resolution of 0.1 μm . All data were collected by the dynamic signal analyzer. It is noted that each sample was subject to a mechanical preload of 3.5 MPa along the $[001]$ direction for 3 min prior to a magnetomechanical test. This preloading process reset any multivariant states to an initial nearly single-variant state in the sample, thus allowing for a direct comparison of all mechanical loading conditions to be discussed in Figs. 2 and 3.

Figure 2 shows the MFISs of Ni–Mn–Ga single crystal and its multilayer and sandwich composites under different applied mechanical loads (σ) for the first one and a quarter cycles of the applied magnetic field (H). Figure 2(a) also includes various illustrations, depicting the evolution of twin

variants at load-free ($\sigma=0$ MPa) condition for the single crystal. Referring to the load-free case in Fig. 2(a), the yellow region with an arrow “ \rightarrow ” in illustration O represents the initial nearly single-variant state (state I). By positively increasing H to ~ 350 kA/m, there is no obvious increase in MFIS due to the pinning of twin boundary. Once H is increased beyond this critical value, an easy reversible reorientation of twin variants is initiated and a new variant state appears and grows rapidly at the expense of the other as indicated by the darker region with an arrow “ \uparrow ” in illustration A, resulting in a rapid increase in MFIS. Further increasing H to 720 kA/m causes the new variant state to grow to a new nearly single-variant state (state II) as in illustration B, leading to a saturation MFIS of 5.6%. When H is reduced back to zero (at remanence), state II is almost preserved by the irreversible reorientation of twin variants as shown in illustration C, giving a gradual decrease in MFIS with a remanent strain of 5.3%. By applying a negative H , there is a 180° rotation in magnetization vectors associated with the two variant states in illustration D compared to illustration C. Further increasing the negative H to saturation at -720 kA/m makes the variant state having the green region with an arrow “ \downarrow ” in illustration D to grow to a nearly single-variant state similar to state II but with an opposite magnetization vector, as displayed in illustration E. A subsequent cycling H recovers the MFIS curve depicted by illustrations B, C, D, E, etc. For the loaded cases in Fig. 2(a), while the MFIS curves exhibit a strong dependence on σ , they have similar quantitative trends to the load-free case described above. However, a distinct difference is observed for the ones with $\sigma \geq 2.5$ MPa in that the MFISs are fully reversible without remanent strain. For the multilayer composite in Fig. 2(b) and sandwich composite in Fig. 2(c), although the load-free MFISs are only partially reversible, the loaded ones become fully reversible at much reduced σ of 1.5 and 1.2 MPa, respectively.

To better understand the effect of σ on MFISs, we regard the first quarter cycle and subsequent one cycle of MFISs in Fig. 2 as the dc- and ac-MFISs, respectively, and plot the dependences of dc-MFIS, remanent strain, and ac-MFIS on σ in Fig. 3 for Ni–Mn–Ga single crystal and its multilayer and sandwich composites. Here, we reported that dc-MFIS, remanent strain, and ac-MFIS values are the MFIS values at saturation, at remanence, and between saturation and remanence, respectively. From Fig. 3, it is clear that the load-free dc-MFIS drops from 5.6% to 1.5% in the multilayer composite and to 0.8% in the sandwich composite as a result of the decreased Ni–Mn–Ga volume fraction and the increased stress bias of the Ni–Mn–Ga plates by the PU plates. For all samples, the monotonic decrease in dc-MFIS with the increase in σ reflects the use of magnetic field energy to overcome the increased mechanical load energy rather than to facilitate a reorientation of twin variants. As σ is elevated to a certain level, the reorientation of twin variants is completely inhibited. That is, the dc-MFIS is completely blocked at 3.5, 3.0, and 2.5 MPa for the single crystal, multilayer composite, and sandwich composite, respectively. This

means that a 3.5 MPa preload is large enough to block all our samples and to reset any multivariant states to an initial nearly single-variant state [e.g., illustration O in Fig. 2(a)]. This is further evident by the excellent agreement between the theoretical maximum lattice strain of 5.7%, the measured load-free dc-MFIS of 5.6%, and the manufacturer’s load-free dc-MFIS of 5.6% in the single crystal. Thus, this 3.5 MPa preload was used to reset all our samples prior to a magneto-mechanical test. Similar to dc-MFISs, the remanent strain decreases with the increase in σ and becomes zero at 2.5, 1.5, and 1.2 MPa for the single crystal, multilayer composite, and sandwich composite, respectively. In fact, the main difference between the single crystal and the composites is their ac-MFISs. For the single crystal in Fig. 3(a), the ac-MFIS increases initially from the load-free value of 0.3%, peaks at 1.6 MPa with a value of 3%, and then decreases with increasing σ . The multilayer and sandwich composites in Figs. 3(b) and 3(c) demonstrate similar gradual decreasing trends in ac-MFIS with increasing σ to the dc-MFISs with load-free values of 0.8% and 0.5%, respectively. Although the dc-MFISs in composites are much smaller than the single crystal, their load-free ac-MFISs are comparatively larger and can provide significant cyclic strains for actuator and transducer applications without the aid of σ .

We have fabricated FSM composites of multilayer and sandwich types based on plate-shaped Ni–Mn–Ga single crystal and PU polymer besides investigating their dc- and ac-MFISs as functions of both magnetic field and mechanical load in conjunction with the single crystal. All samples have demonstrated a strong dependence of MFIS on the applied mechanical load. The multilayer and sandwich composites have relatively lower load-free dc-MFISs but higher load-free ac-MFISs than the single crystal due to the stress bias of the Ni–Mn–Ga plates by the PU plates in the composites. The enhanced load-free ac-MFISs in the composites indicate great potential for actuator and transducer applications without the application of mechanical load.

This work was supported by the Hong Kong Research Grants Council of the HKSAR Government (Grant No. PolyU 5257/06E, and N-PolyU 501/08) and The Hong Kong Polytechnic University (Grant No. A-PA3C).

¹K. Ullakko, J. K. Huang, C. Kantner, R. C. O’Handley, and V. V. Kokorin, *Appl. Phys. Lett.* **69**, 1966 (1996).

²S. J. Murray, M. Marioni, S. M. Allen, R. C. O’Handley, and T. A. Lograsso, *Appl. Phys. Lett.* **77**, 886 (2000).

³A. Sozinov, A. A. Likhachev, N. Lanska, and K. Ullakko, *Appl. Phys. Lett.* **80**, 1746 (2002).

⁴T. Sakamoto, T. Fukuda, T. Kakeshita, T. Takeuchi, and K. Kishio, *J. Appl. Phys.* **93**, 8647 (2003).

⁵K. Oikawa, T. Ota, T. Ohmori, Y. Tanaka, H. Morito, A. Fujita, R. Kainuma, K. Fukamichi, and K. Ishida, *Appl. Phys. Lett.* **81**, 5201 (2002).

⁶H. Morito, A. Fujita, K. Fukamichi, R. Kainuma, K. Ishida, and K. Oikawa, *Appl. Phys. Lett.* **81**, 1657 (2002).

⁷C. P. Henry, D. Bono, J. Feuchtwangler, S. M. Allen, and R. C. O’Handley, *J. Appl. Phys.* **91**, 7810 (2002).

⁸M. Zeng, S. W. Or, and H. L. W. Chan, *J. Alloys Compd.* **490**, L5 (2010).

⁹E. Gans and G. P. Carmen, *J. Appl. Phys.* **99**, 084905 (2006).